Supplementary Information: Efficient photon-pair generation in layer-poled lithium niobate nanophotonic waveguides

Xiaodong Shi,[1,a] Sakthi Sanjeev Mohanraj,[1,a] Veerendra Dhyani,[1] Angela Anna Baiju,[1,2] Sihao Wang,[1] Jiapeng Sun,[3] Lin Zhou,[4] Anna Paterova,[1] Victor Leong,[1] and Di Zhu[1,3,4,b]

[1] *A*STAR Quantum Innovation Centre (Q.InC), Institute of Materials Research and Engineering (IMRE), Agency for Science, Technology and Research (A*STAR), 138634, Singapore*

[2] *Department of Physics, National University of Singapore, 117542, Singapore*

[3] *Department of Materials Science and Engineering, National University of Singapore, Singapore 117575, Singapore*

[4] *Centre for Quantum Technologies, National University of Singapore, Singapore 117543, Singapore*

(Dated: May 30, 2024)

[a] These authors contributed equally.

[b] Electronic mail: dizhu@nus.edu.sg

I. SUPPLEMENTARY FIGURES

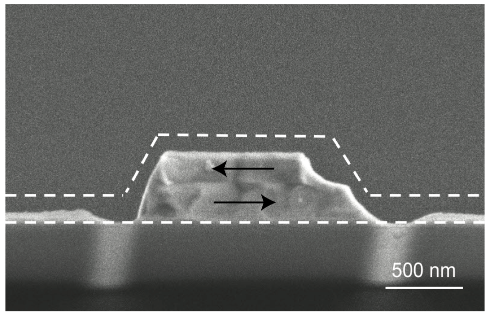

FIG. S1. Scanning electron micrograph of the LPLN waveguide cross-section after intentional anisotropic wet etching. A clear boundary between the two domains and the discontinuity of their sidewalls can be observed, indicating layer-wise inverse polarities. The white dashed line marks the original LPLN waveguide cross-section before wet etching.

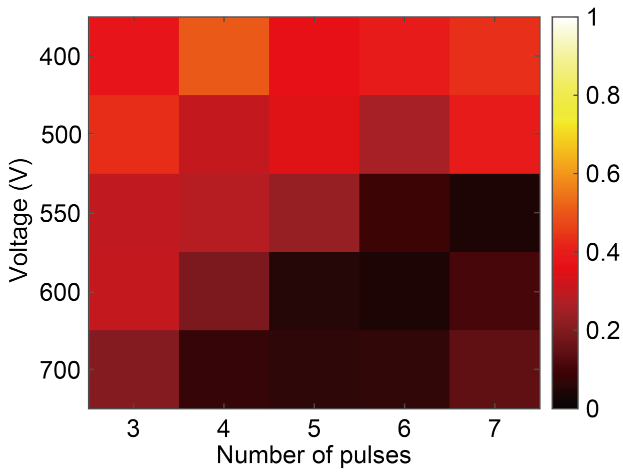

FIG. S2. Relation between poling depth and poling conditions (poling voltage and number of pulses). Instead of directly visualizing each device's cross-section, we use the count rates from the confocal SHG imaging (see Fig. 1f in main text) to infer the poling depth. Here, the colorbar is the ratio between the SHG signals in the poled and unpoled waveguides. A high ratio indicates weak spatial symmetry breaking in the poled waveguides (i.e., close to being completely unpoled or fully poled), and a low ratio indicates strong layer-wise symmetry breaking (i.e., partially poled) due to the destructive interference between the two inversely polarized layers. There is a reasonable margin for the selection of voltage and number of pulses to achieve the desired partial poling. The poling is performed after waveguide etching and at room temperature. We choose 6 pulses with 600 V voltage for the final device fabrication.

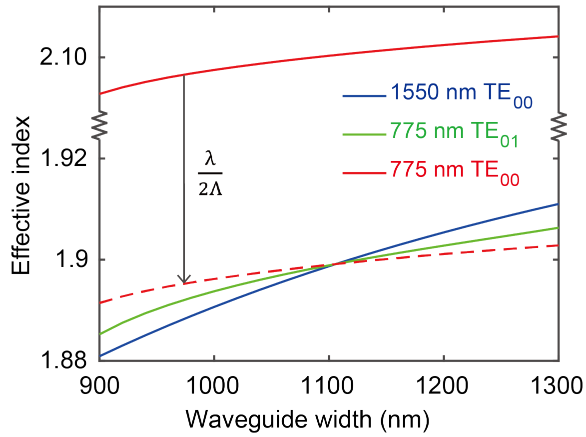

FIG. S3. Simulation of effective indices of the TE_{00} mode at 1550 nm (blue), the TE_{00} mode at 775 nm (red), and the TE_{01} modes at 775 nm (green) as a function of LN waveguide width. As the waveguide width increases, the effective index of the FH TE_{00} mode exhibits a slower rate of increase compared to that of the SH TE_{01} mode. The intersection point at $\sim$1100 nm between the blue and green curves signifies the phase-matching point for MPM. A larger slope difference between the FH TE_{00} and SH TE_{00} modes is seen compared to that between FH TE_{00} and SH TE_{01} modes, indicating that QPM in PPLN is more sensitive than MPM in LPLN in terms of the waveguide width variation. Here, the $\lambda/2\Lambda$ shift indicates momentum matching offered by QPM in PPLN.

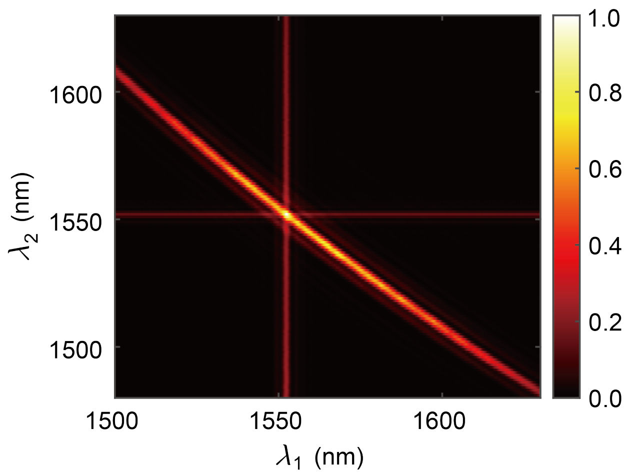

FIG. S4. Sum-frequency generation (SFG) phase-matching function from 1480 nm to 1630 nm, measured by sweeping two telecom cw lasers and measuring the generated SFG power. The diagonal slope follows the energy conservation line ($1/\lambda_1 + 1/\lambda_2 = 1/\lambda_{\mathrm{SHG}}$), allowing broadband SPDC.

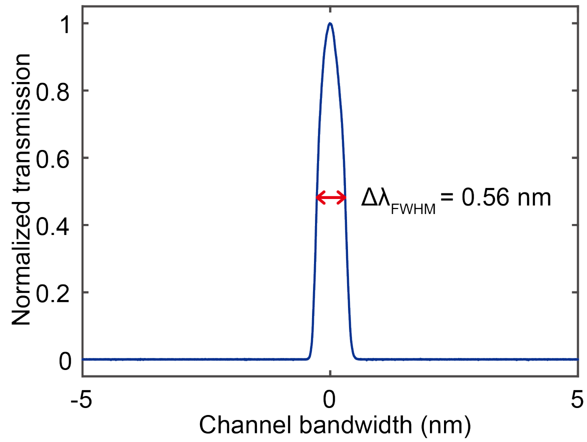

FIG. S5. Measured transmission spectrum of the signal/idler channel used in the photon-pair measurement, showing a FWHM bandwidth of 0.56 nm. This bandwidth is used to calculate the SPDC brightness.

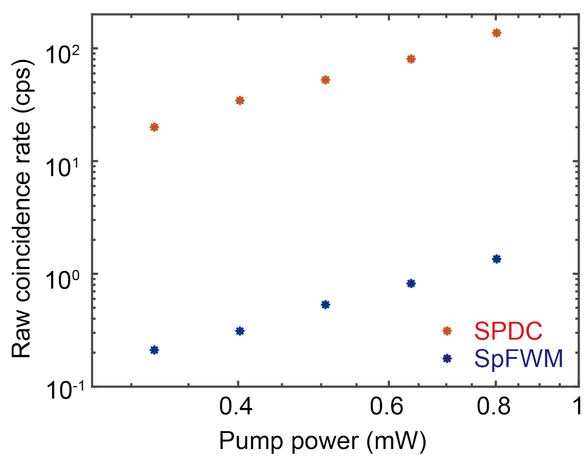

FIG. S6. Measured off-chip, raw photon-pair generation rates from SPDC (red) and SpFWM (blue) as a function of on-chip pump power. The PGR from SPDC is about two orders of magnitude higher than that from SpFWM.

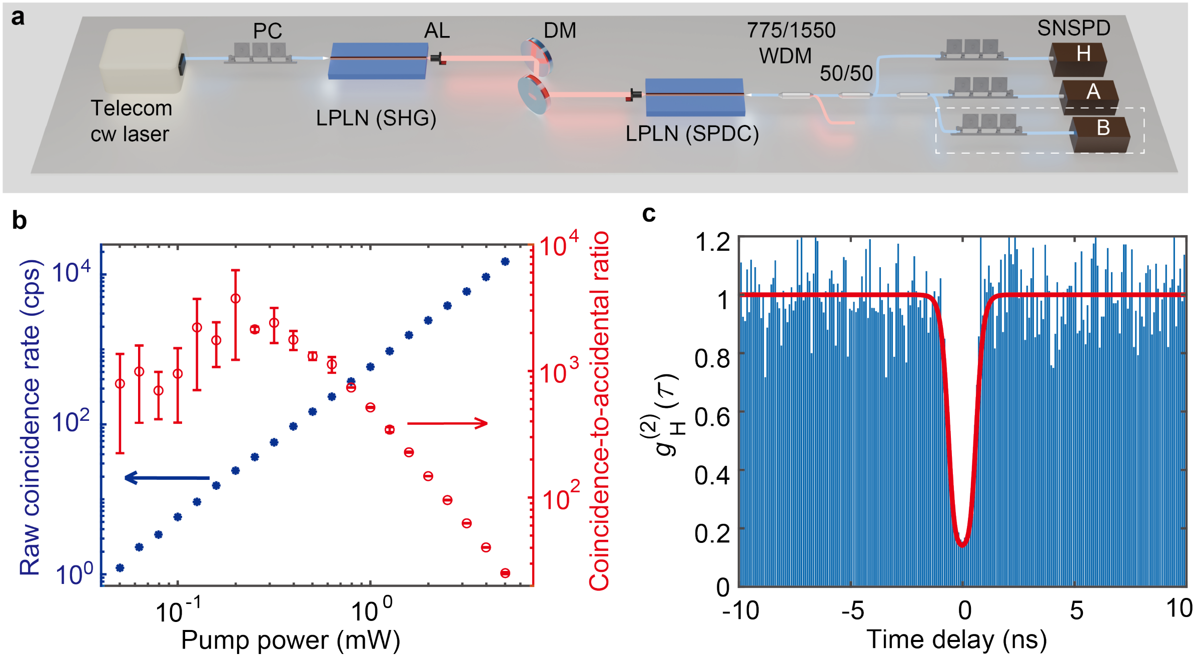

FIG. S7. Photon-pair generation with two LPLN chips, one for SHG and the other for SPDC. **a**, Experimental setup. The SH light, generated in the first chip, is coupled out from the first chip and then into the second chip through a pair of aspheric lenses (AL). The telecom pump light is filtered in between using dichroic mirrors (DM). SPDC photon pairs generated in the second chip is coupled out using a lensed fiber, and the SH light is filtered out through a 1550 nm/775 nm WDM. Signal and idler photons are separated using a 50/50 beamsplitter and sent to SNSPDs for coincidence counting with H and A, and heralded second-order correlation function measurement with H, A, and B. **b**, Off-chip, raw measured photon-pair generation rate (blue) and CAR (red) versus on-chip pump power. **c** Measured (blue) and fitted (red) heralded second-order correlation function versus time delay at a pump power of 5.0 mW, and it is measured to be 0.014 at zero time delay, indicating the measurements are operated in the single-photon regime.

II. SCALING LAWS FOR CASCADED SHG AND SPDC PROCESS

In this section, we use a simplified classical model to derive the scaling laws for the cascaded SHG-SPDC photon-pair generation process. We note that this model does not capture the quantum nature of SPDC and is not sufficient to predict the absolute photon-pair generation rate or dynamics. In a cascaded SHG and non-degenerate SPDC process based on MPM without phase mismatch, the coupled amplitude differential equation can be expressed as

$$\frac{\partial A_1}{\partial z} = i\frac{\omega_1^2}{c^2 k_1} d_{\mathrm{eff}} A_1^*(z) A_2(z), \tag{1}$$

$$\frac{\partial A_2}{\partial z} = i\frac{\omega_2^2}{c^2 k_2} d_{\mathrm{eff}} A_1(z) A_1(z) + i\frac{\omega_2^2}{c^2 k_2} d_{\mathrm{eff}} A_{\mathrm{s}}(z) A_{\mathrm{i}}(z), \tag{2}$$

$$\frac{\partial A_{\mathrm{s}}}{\partial z} = i\frac{\omega_{\mathrm{s}}^2}{c^2 k_{\mathrm{s}}} d_{\mathrm{eff}} A_{\mathrm{i}}^*(z) A_2(z), \tag{3}$$

$$\frac{\partial A_{\mathrm{i}}}{\partial z} = i\frac{\omega_{\mathrm{i}}^2}{c^2 k_{\mathrm{i}}} d_{\mathrm{eff}} A_{\mathrm{s}}^*(z) A_2(z), \tag{4}$$

where ω and k are frequency and wavevector, respectively, and the indices 1, 2, s, and i indicate the parameters at FH, SH, signal and idler frequencies, respectively. Following energy conservation, we have $\omega_2 = 2\omega_1$ and $\omega_2 = \omega_{\mathrm{i}} + \omega_{\mathrm{s}}$. Furthermore, we assume the FH pump is in a non-depletion regime, and the FH and SH fields are much stronger than the signal and idler fields. Hence, A_1 can be treated as a constant, and Eq. 2 is simplified to

$$\frac{\partial A_2}{\partial z} = i\frac{\omega_2^2}{c^2 k_2} d_{\mathrm{eff}} A_1 A_1. \tag{5}$$

Combining Equations 3-5, we have

$$\frac{\partial^2 A_{\mathrm{s}}}{\partial z^2} - \frac{1}{z}\frac{\partial A_{\mathrm{s}}}{\partial z} - \frac{z^2}{g^4} A_{\mathrm{s}} = 0, \tag{6}$$

where $g = \frac{(k_1^2 k_{\mathrm{i}} k_{\mathrm{s}})^{1/4} c^2}{(\omega_{\mathrm{s}}\omega_{\mathrm{i}})^{1/2}\omega_2 d_{\mathrm{eff}} A_1}$. Eq. 6 has a general solution in the form of

$$A_{\mathrm{s}}(z) \propto C_1 \sinh(z^2/2g^2) + C_2 \cosh(z^2/2g^2) \propto z^2/2g^2 + \mathcal{O}(z^4), \tag{7}$$

where C_1 and C_2 are constants and the last approximation assumes $z \ll g$. For a short waveguide of length L, we can expect the SPDC rate in the cascaded SHG-SPDC process to scale as $P_{\mathrm{s}} \propto P_1^2 L^4$, where $P_{\mathrm{s}} = |A_{\mathrm{s}}|^2$ and $P_1 = |A_1|^2$. The quadratic relation between the photon-pair generation rate and the pump power agrees well with the measurement in Fig. **??**c. The quartic relation between the signal power and the propagation length indicates that increasing the waveguide length is an effective means to further increase the pair generation efficiency. As a comparison, the photon-pair generation rate in standard SPDC with SH pump scales as $\propto P_{\mathrm{pump}} L^2$, and that in SpFWM with telecom pump scales as $\propto P_{\mathrm{pump}}^2 L^2$.